ISSN 1674-1056
http://cpb.iphy.ac.cn
http://iopscience.iop.org/cpb
中国物理 B
Chinese Physics
中国物理 Chinese Physics B

Key parameters of two typical intercalation reactions to prepare hybrid inorganic-organic perovskite films

Biao Shi(石标), Sheng Guo(郭升), Changchun Wei(魏长春), Baozhang Li(李宝璋), Yi Ding(丁毅), Yuelong Li(李跃龙), Qing Wan(万青), Ying Zhao(赵颖), Xiaodan Zhang(张晓丹)
Citation: Chin. Phys. B . 2018, 27(1): 018807. **doi:** 10.1088/1674-1056/27/1/018807

Journal homepage: http://cpb.iphy.ac.cn; http://iopscience.iop.org/cpb

What follows is a list of articles you may be interested in

---

420 nm thick $CH_3NH_3PbI_{3-x}Br_x$ capping layers for efficient TiO_2 nanorod array perovskite solar cells

Long Li(李龙), Cheng-Wu Shi(史成武), Xin-Lian Deng(邓新莲), Yan-Qing Wang(王艳青), Guan-Nan Xiao(肖冠南), Ling-Ling Ni(倪玲玲)
Chin. Phys. B . 2018, 27(1): 018804. **doi:** 10.1088/1674-1056/27/1/018804

Promise of commercialization:carbon materials for low-cost perovskite solar cells

Yu Cai(蔡宇), Lusheng Liang(梁禄生), Peng Gao(高鹏)
Chin. Phys. B . 2018, 27(1): 018805. **doi:** 10.1088/1674-1056/27/1/018805

O_3 fast and simple treatment-enhanced p-doped in Spiro-MeOTAD for CH_3NH_3I vapor-assisted processed $CH_3NH_3PbI_3$ perovskite solar cells

En-Dong Jia(贾恩东), Xi Lou(娄茜), Chun-Lan Zhou(周春兰), Wei-Chang Hao(郝维昌), Wen-Jing Wang(王文静)
Chin. Phys. B . 2017, 26(6): 068803. **doi:** 10.1088/1674-1056/26/6/068803

Simulation design of P-I-N-type all-perovskite solar cells with high efficiency

Hui-Jing Du(杜会静), Wei-Chao Wang(王韦超), Yi-Fan Gu(顾一帆)
Chin. Phys. B . 2017, 26(2): 028803. **doi:** 10.1088/1674-1056/26/2/028803

Device simulation of lead-free $CH_3NH_3SnI_3$ perovskite solar cells with high efficiency

Hui-Jing Du(杜会静), Wei-Chao Wang(王韦超), Jian-Zhuo Zhu(朱键卓)
Chin. Phys. B . 2016, 25(10): 108802. **doi:** 10.1088/1674-1056/25/10/108802

SPECIAL TOPIC — New generation solar cells

Key parameters of two typical intercalation reactions to prepare hybrid inorganic–organic perovskite films*

Biao Shi(石标)[1,2,3,4], Sheng Guo(郭升)[1,2,3,4], Changchun Wei(魏长春)[1,2,3,4], Baozhang Li(李宝璋)[1,2,3,4], Yi Ding(丁毅)[1,2,3,4], Yuelong Li(李跃龙)[1,2,3,4], Qing Wan(万青)[5], Ying Zhao(赵颖)[1,2,3,4], and Xiaodan Zhang(张晓丹)[1,2,3,4,†]

[1] *Institute of Photoelectronic Thin Film Devices and Technology, Nankai University, Tianjin* 300071, *China*
[2] *Key Laboratory of Photoelectronic Thin Film Devices and Technology of Tianjin, Tianjin* 300071, *China*
[3] *Key Laboratory of Optical Information Science and Technology of Ministry of Education, Tianjin* 300071, *China*
[4] *Collaborative Innovation Center of Chemical Science and Engineering (Tianjin), Tianjin* 300072, *China*
[5] *College of Electronic Science and Engineering, Nanjing University, Nanjing* 210093, *China*

(Received 6 October 2017; revised manuscript received 24 November 2017; published online 13 December 2017)

A star hybrid inorganic–organic perovskite material selected as an outstanding absorbing layer in solar cells benefits from multiple preparation techniques and excellent photoelectric characteristics. Among numerous synthetic processes, uniform, compact, and multi-stack perovskite thin films can be manufactured using vacuum deposition. During sequential vacuum deposition, the penetration ability of the organic molecules cannot be effectively controlled. In addition, the relationship between the thickness of the inorganic seeding layer and the organic molecule concentration for optimized devices using an evaporation–solution method is unclear. In this work, we prepared high-quality perovskite films by effectively controlling the penetration ability and chemical quantity of organic methyl ammonium iodide by monitoring the evaporation pressure and time. Thus, a device efficiency of over 15% was achieved with an all-vacuum prepared perovskite film. For the evaporation–solution method, we reacted different thicknesses of inorganic lead iodine with various concentrations of the organic molecule solution. The inorganic layer thickness and organic molecule concentration showed a linear relationship to achieve an optimum perovskite film, and an empirical formula was obtained. This work noted the key parameters of two intercalation reactions to prepare perovskite films, which paves a way to deliver a device that enables multi-layered structures, such as tandem solar cells.

Keywords: perovskite solar cell, sequential vacuum deposition, evaporation–solution method, intercalation reaction

PACS: 88.40.H–, 88.40.hj, 88.40.fh, 91.60.Ed **DOI:** 10.1088/1674-1056/27/1/018807

1. Introduction

Hybrid organic–inorganic perovskite materials have attracted tremendous attention due to their excellent properties, such as large charge carrier mobility,[1] long diffusion length,[2] high absorption coefficient,[3,4] tunable band gap,[5–8] and unique tolerance to structural defects.[9,10] The outstanding optoelectronic characteristics combined with multiple manufacturing methods[11–19] have presented such materials with extensive applications in light emitting devices (LEDs),[20,21] thin film transistors (TFTs),[22] photodetectors,[23,24] solar cells,[25–28] and others. During preparation, a distinct advantage of vacuum deposition over solution processing is the ability to prepare layered uniform, compact, and multi-stack thin films,[15] which enables multi-layered structures. However, the efficiencies are lower and successful cases of efficiencies over 15% are few for vacuum deposited solar cells[15,29] compared to solar cells prepared with solution processing,[30] which mainly results from the small density and high vapor pressure of organic methyl ammonium iodide (MAI) diffusing inside the vacuum chamber, making it very difficult to control the ratio of organic MAI to inorganic lead salt.[31–34] To improve the controllability during vacuum deposition, inorganic lead halides and organic MAI have been prepared in separated processes to synthesize perovskite films, as shown in the scheme in Fig. 1(a). Vapor-assisted solution processing,[16,35,36] sequential vacuum deposition,[37,38] evaporation–solution processing,[39–45] hybrid chemical vapor deposition,[46] layer-by-layer growth,[47] and alternating precursor layer deposition[48] have been developed and can enhance the experimental repeatability, as these preparation routes can provide strict control over the stoichiometry of organic MAI vapor. However, as common methods of control, monitoring the organic vapor rate with quartz monitor crystals[36,48] or evaporating organic halide at a fixed

*Project supported by the International Cooperation Project of the Ministry of Science and Technology, China (Grant No. 2014DFE60170), the National Natural Science Foundation of China (Grant Nos. 61474065 and 61674084), Tianjin Research Key Program of Application Foundation and Advanced Technology, China (Grant No. 15JCZDJC31300), Key Project in the Science & Technology Pillar Program of Jiangsu Province, China (Grant No. BE2014147-3), and the 111 Project, China (Grant No. B16027).

†Corresponding author. E-mail: xdzhang@nankai.edu.cn

© 2018 Chinese Physical Society and IOP Publishing Ltd

temperature[32] are invalid for controlling the penetration ability of the randomly diffused organic halide vapor. In addition, the relationship between the thickness of the inorganic lead halide layer and the concentration of MAI/isopropyl alcohol (IPA) for optimized device performance is unclear, which is vital for evaporation–solution methods widely used in semi-transparent and tandem devices.[40–42,49,50]

In fact, an intercalation process is required to manufacture a perovskite film with a step-by-step deposition process.[51–53] During the organic molecule penetration process into the inorganic skeleton, the thickness of the inorganic seeding layer and the penetration ability and chemical quantity of the organic molecules are core factors. Heating the substrate has been shown as a successful method to enhance the penetration ability of organic MAI molecules.[37] In our work, first, we prepared a high-quality perovskite film by controlling the penetration ability and chemical quantity of the MAI vapor through monitoring the evaporation pressure and time. The efficiency of the perovskite solar cell (PSC) reached over 15% with the all-vacuum prepared perovskite film. Moreover, the thickness of the inorganic lead halide and the concentration of the organic molecule solution show a linear relationship with the optimized perovskite film, and an empirical formula was proposed for the evaporation–solution method.

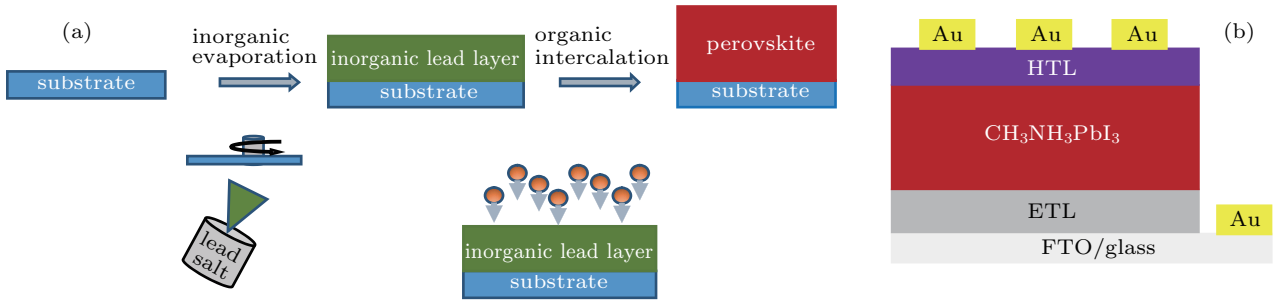


Fig. 1. (color online) Scheme illustration of the intercalation reaction to form the perovskite film and schematic structure of the PSC. (a) First, the inorganic lead halide was sublimed, and then, the as-deposited inorganic seeding layer was reacted with organic molecules through a penetration process. (b) Schematic structure of the PSC with the perovskite film prepared by sequential vacuum deposition and evaporation–solution methods.

2. Experimental section

2.1. Substrate cleaning and HTL precursor preparation

Transparent conductive fluorine-doped tin oxide (FTO)/glass (13 Ω/□) films were purchased from Lattice Solar Energy Technology Co. Ltd. in Wuhan. The FTO/glass substrates were first sequentially cleaned with a semiconductor industrial cleaner (Huaxing DZ-1, Jinan Xihua Technology Co. Ltd) and deionized water in an ultrasonic bath for 50 min and then dried using nitrogen gas. A chlorobenzene solution (1 mL) containing 2,2′,7,7′-tetrakis(N,N′-di-p-methoxyphenylamine)-9,9′-spirobifluorene (spiro-OMeTAD, 80 mg), 4-tert-butylpyridine (TBP, 28.5 μL) and a lithium bis(trifluoromethylsulfonyl)imide (LiTFSI, 17.5 μL) solution (520 mg LiTFSI in 1 mL of acetonitrile) were prepared for the organic hole transporting layer (HTL).

2.2. Cells with perovskite films manufactured by sequential vacuum deposition

A TiO_2 film with a thickness of ∼ 50 nm was deposited on top of the FTO/glass substrate by DC magnetron sputtering. Then, the substrate was transferred into a vacuum system (Kurt J. Lesker, Britain). After the base pressure of the system was pumped down to 5×10^{-6} Torr, $PbCl_2$ evaporation was initiated by heating the crucible, and the evaporation rate of $PbCl_2$ was precisely maintained at 2 Å/s under careful monitoring by a quartz crystal. The heating of the $PbCl_2$ crucible was immediately stopped when the thickness on the quartz crystal reached 3.6 kÅ, which resulted in a $PbCl_2$ film with an actual thickness of 100 nm. After cooling the $PbCl_2$ crucible for 5 min, a crucible with MAI was slowly heated until the chamber pressure reached the required pressure, and the evaporation temperature was maintained over time. The as-deposited films were annealed at 100 °C for 30 min in a N_2-filled glove box. Then, 20 μL of a spiro-OMeTAD solution was spin coated on the perovskite films at 6000 rpm for 30 s. Finally, a 100 nm gold layer was thermally evaporated on top of the HTL to complete the device.

2.3. Cells with perovskite films manufactured by an evaporation–solution method

First, a 12 nm TiO_2 film with titanium isopropoxide (TTIP) and oxygen plasma as precursors was deposited onto the FTO/glass by atomic layer deposition (ALD) (Model: SI ALD, Company: SENTECH). Then, 50 μL of a 10 mg/mL [6,6]-phenyl C_{61}-butyric acid methyl ester ($PC_{61}BM$)/chlorobenzene (CB) solution was spin coated onto the TiO_2/FTO/glass substrates at 3500 rpm for 30 s. Different thicknesses of PbI_2 were subsequently deposited on the substrates by evaporation. The base pressure of the system was 3×10^{-6} Torr, and the evaporation rate was 2 Å/s. The substrates coated with PbI_2 films were taken into a glove box without exposure to air. MAI/IPA solutions with various concentrations were loaded on the PbI_2 film for 1 min before rotating the substrates at 2000 rpm for 40 s and then annealing the films at 140 °C for 25 min. Then, 70 μL of a spiro-OMeTAD solution was spin coated on the perovskite films at 4000 rpm

for 60 s. Finally, a 100 nm gold layer was thermally evaporated on top of the HTL to complete the device.

2.4. Film and device characterization

The PbI_2 thickness was measured with a microfigure measuring instrument (Surfcorder ET200, Kosaka Laboratory Ltd). The morphologies of the perovskite films were characterized using scanning electron microscopy (SEM) (JEOL JSM-6700F). X-ray diffraction (XRD, Rigaku ATX-XRD) patterns of the perovskite films were obtained using Cu $K\alpha$ radiation as the radiation source ($\lambda = 1.5405$ Å) across a 2θ range of 5° to 70°. Time-resolved photoluminescence (TRPL) spectroscopy was measured with a PL spectrometer (Edinburgh Instruments, FLS 920), and a pulsed laser with a wavelength of 635 nm and a repetition rate of 1 MHz was employed as the excitation source. A 655 nm filter was used to filter out the excitation light. Photocurrent density–voltage (J–V) curves of the solar cells were measured from 1200 mV to −200 mV (forward bias to short circuit (FB-SC)) and returned (SC-FB) with a voltage step of 40 mV and delay time of 50 ms at 25 °C in a N_2-filled glovebox. A metal mask with a window of 0.1 cm^2 was coated on the light incident side to define the active area of the cell. A solar simulator (HAL-320, ASAHI SPECTRA Co. Ltd., Japan) with a compact xenon light source was used to produce the simulated AM 1.5G irradiation (100 mW/cm^2), and the calibration of the light was carried out by a detector (CS-20, ASAHI SPECTRA Co. Ltd., Japan) with a silicon reference cell. The external quantum efficiency (EQE) spectral response was measured with a QEX10 (PV measurement).

3. Results and discussion

The perovskite film was manufactured with sequential vacuum deposition,[37,54] and the detailed process has been described in the experimental section. A 100 nm inorganic $PbCl_2$ seeding layer was first sublimed onto the substrate with a controlled rate. In addition to the concentration and temperature, the pressure of the organic MAI vapor was manipulated to realize an effective diffusion reaction. The grain size at a low organic vapor pressure (Fig. 2(a), 5×10^{-5} Torr) was smaller than that at a high vapor pressure (Figs. 2(b) and 2(c), 1.5×10^{-4} Torr). The three XRD peaks of $CH_3NH_3PbI_3$ ($MAPbI_3$) corresponding to the (110), (220), and (330)[15,55] lattice planes were stronger and shaper at an organic vapor pressure of 1.5×10^{-4} Torr, as shown in Fig. 2(d), indicating the formation of larger perovskite grains. The increased crystalline grain size of the perovskite at high pressure was attributed to the improved reaction rate of $PbCl_2$ and MAI,[36] referred to as Ostwald ripening.[56,57] At high MAI vapor pressure, more and higher-reactive MAI molecules will react with $PbCl_2$, which favors secondary nucleation at the primary sites. The nucleation sites of the large crystallites grow faster because of the larger contact area. As a result, the larger crystalline grains grow even larger and diminish the small perovskite nucleation sites. Therefore, a suitable high pressure of organic MAI is beneficial for the formation of high-quality perovskite films.

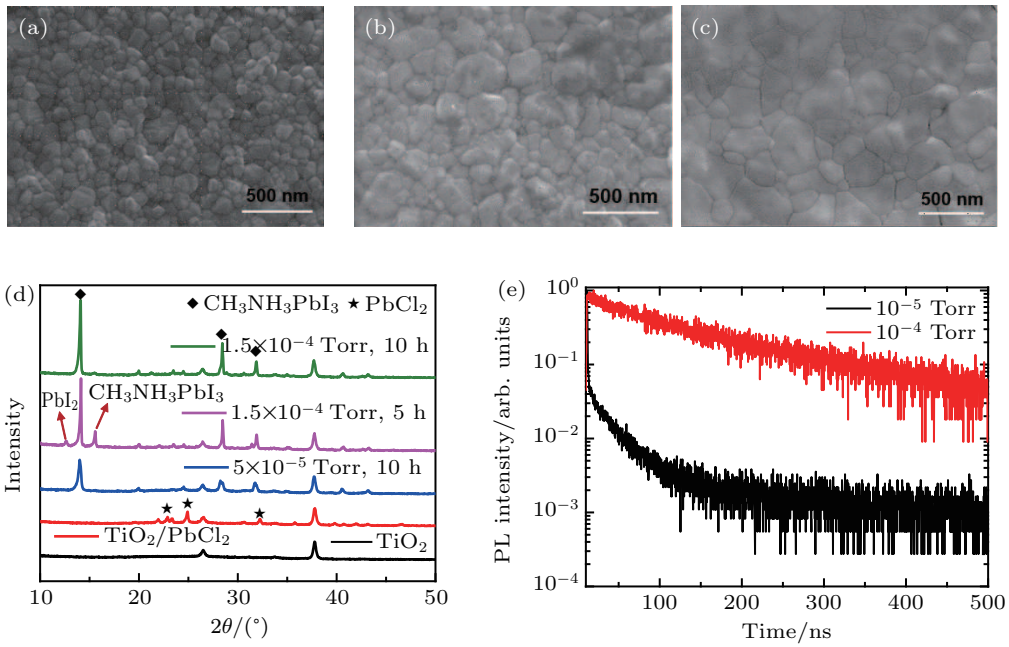


Fig. 2. (color online) Surface morphology, phase, and electrical properties of the perovskite film prepared by sequential vacuum deposition before annealing. SEM top-view images of the perovskite films prepared with various organic MAI sublimation pressures and duration time: (a) 5×10^{-5} Torr, 10 h; (b) 1.5×10^{-4} Torr, 5 h; (c) 1.5×10^{-4} Torr, 10 h. (d) XRD patterns of the perovskite films prepared with various sublimation conditions of organic MAI. (e) TRPL spectroscopy of the FTO/TiO_2/perovskite film prepared with a MAI vapor pressure of 10^{-4} Torr or 10^{-5} Torr. The inorganic seeding layer is 100 nm $PbCl_2$. The sublimation duration time of organic MAI reflects its chemical quality and is sufficient when the time is 10 h but insufficient at 5 h.

Transient TRPL decay measurements were conducted to investigate the electrical properties of the perovskite film (Fig. 2(e)). A single-exponential function $(A+B_1\exp(-t/\tau_1))$ was used to fit the PL decay time. The decay time of the sample with an organic vapor pressure of 10^{-5} Torr is 25.43 ± 0.26 ns, while the decay time of 10^{-4} Torr is 115.69 ± 1.65 ns. The rapid decay for the sample prepared at an organic vapor pressure of 10^{-5} Torr results from the quick recombination in the perovskite bulk caused by more grain boundaries.[58]

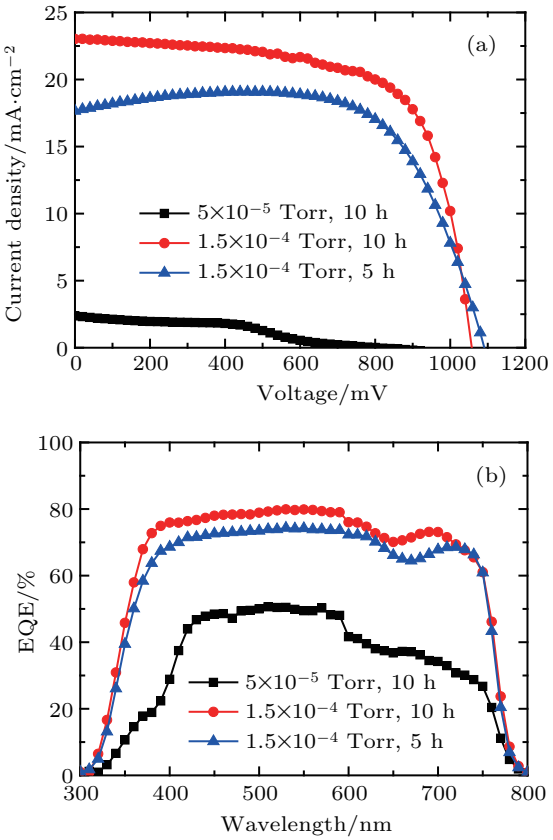


Fig. 3. (color online) Performance of PSCs prepared using sequential vacuum deposition. (a) *J*–*V* characteristics with an effective area of 0.1 cm^2 (FB-SC) under 1 sun illumination and (b) the corresponding EQE curves for PSCs with various thermal evaporation deposition conditions.

The chemical quantity of MAI is also important in the formation of $MAPbI_3$. As shown in Fig. 2(d), the peaks at $2\theta = 12.58^\circ$ and 15.56° corresponding to PbI_2 (001) and $CH_3NH_3PbCl_3$ ($MAPbCl_3$) (100)[15,59] appear at an MAI evaporation time of 5 h, indicating the formation of non-pure $MAPbI_3$. However, pure $MAPbI_3$ can be obtained when prolonging the evaporation time of MAI. Based on previous studies[59–61] and the XRD patterns, the reaction steps are listed as follows:

$$PbCl_2 + MAI \rightarrow PbI_2 + MACl\uparrow, \quad (1)$$

$$MACl + PbCl_2 \rightarrow MAPbCl_3, \quad (2)$$

$$MAI + PbI_2 \rightarrow MAPbI_3, \quad (3)$$

$$MAI + MAPbCl_3 \rightarrow MAPbI_3 + MACl\uparrow. \quad (4)$$

First, reactions (1) and (2) occur. Then, MAI reacts with PbI_2 and $MAPbCl_3$ through reactions (3) and (4), respectively. With an insufficient amount of MAI, PbI_2 and $MAPbCl_3$ cannot be consumed, leaving in $MAPbI_3$. With a sufficient amount of MAI, pure $MAPbI_3$ is formed.

Table 1. PSC parameters with different organic vapor pressures and duration time.

Conditions	J_{sc}/mA·cm^{-2}	V_{oc}/mV	*FF*	Eff./%	R_s/Ω·cm^2
5.0×10^{-5} Torr, 10 h	10.5	850	0.310	2.790	606.9
1.5×10^{-4} Torr, 10 h	22.6	1050	0.686	16.28	4.6
1.5×10^{-4} Torr, 5 h	17.6	1090	0.711	13.63	10.0

The efficiency of a PSC (structural schematic shown in Fig. 1(b)) is optimal only when the perovskite film is formed with a high organic MAI vapor pressure and sufficient MAI content. The *J*–*V* characteristics and corresponding EQE curves are shown in Fig. 3, and the device performance parameters are summarized in Table 1. The current density (J_{sc}) from the *J*–*V* curves was larger than integral J_{sc} from EQE, resulting from lateral collection.[62] The PSC with the absorber formed at an MAI vapor pressure of 1.5×10^{-4} Torr demonstrated higher J_{sc}, open-circuit voltage (V_{oc}), and fill factor (*FF*), which are attributed to the larger perovskite grain size, reducing recombination in the perovskite bulk. The PSC fabricated at an MAI vapor pressure of 1.5×10^{-4} Torr but with an MAI evaporation time of 5 h displayed lower J_{sc}, *FF* and higher V_{oc} than the cell with an MAI evaporation time of 10 h, which may result from PbI_2 and $MAPbCl_3$ reducing the absorption[63] but enhancing the band gap.[64]

For the intercalation reaction of the forming perovskite film, the thickness of the inorganic seeding layer and the concentration of the organic molecules are vital.[18] However, the quantitative relationship between the thickness of the inorganic seeding layer and the concentration of the organic molecules for optimal device performance is unclear. We investigated this relationship via an evaporation–solution method[43] because thermally evaporated PbI_2 is non-destructive to substrates and can be prepared with controlled morphology and thickness, and the concentration of the MAI/IPA solution can be easily changed. PbI_2 layers with thicknesses of 85 nm, 150 nm, 200 nm, 270 nm were prepared, and MAI/IPA solutions with four concentrations were spin coated onto each PbI_2 thickness. The performance parameters of PSCs with different PbI_2 thicknesses and MAI/IPA concentrations are shown in Fig. 4. When PbI_2 possessing each thickness reacts with a particular MAI/IPA solution concentration, the PSC can acquire an optimal performance. Maximum photoelectric conversion efficiencies (PCEs) of 11.88%, 13.99%, 14.91%, and 13.33% were obtained with 85 nm, 150 nm, 200 nm, 270 nm PbI_2 reacting with 16 mg/mL, 27.5 mg/mL, 33 mg/mL, 46.5 mg/mL MAI/IPA, respectively.

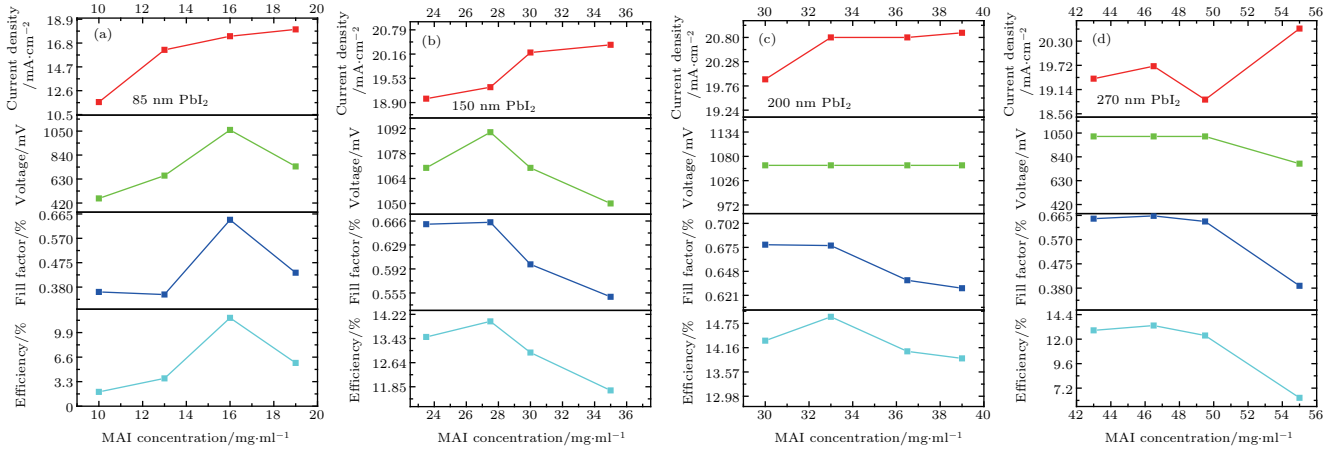


Fig. 4. (color online) Performance parameters of the PSCs prepared using the evaporation–solution method. Performances of the PSCs with PbI_2 thicknesses of (a) 85 nm, (b) 150 nm, (c) 200 nm, and (d) 270 nm reacting with various concentrations of the MAI/IPA solution.

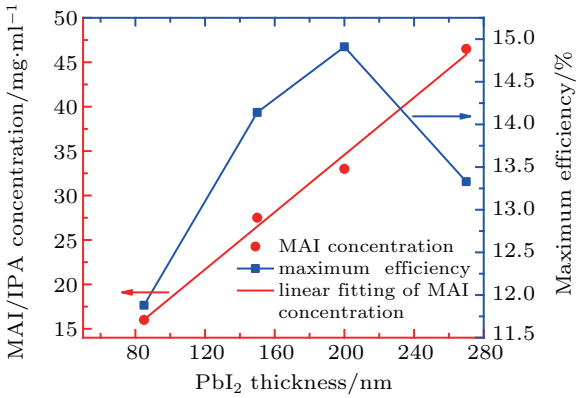


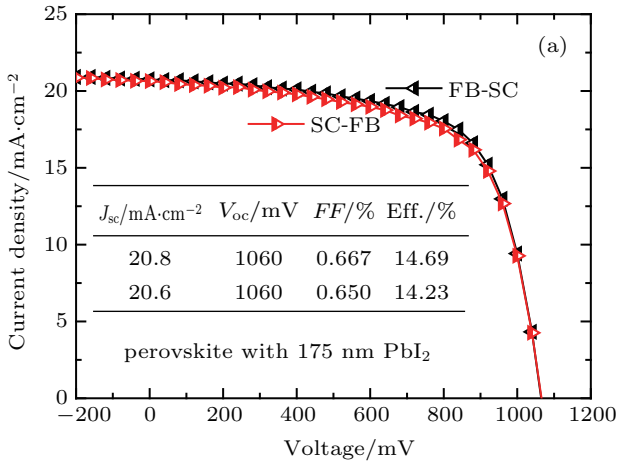
Fig. 5. (color online) Relationship between the PbI_2 thickness and MAI/IPA concentration to achieve the highest PSC efficiency. The thickness of the PbI_2 film has a linear correlation with the MAI/IPA concentration to achieve the optimum perovskite film.

The optimum matching of the MAI/IPA concentration with the PbI_2 thickness is depicted in Fig. 5. Obviously, the optimum MAI/IPA concentration to acquire the maximum PSC efficiency linearly increases with the PbI_2 thickness, and the linear formula fit to the MAI/IPA concentration versus PbI_2 thickness data is

$$y = 0.161x + 2.34, \tag{5}$$

where y is the MAI/IPA concentration, and x is the PbI_2 thickness. To examine the feasibility of the above formula, we prepared 175 nm PbI_2 and reacted the deposited film with 25 mg/mL, 28 mg/mL, 31 mg/mL, and 35 mg/mL MAI/IPA. According to the above formula, the optimum match is 175 nm PbI_2 reacting with 30.5 mg/mL MAI/IPA. Within the margin of error, the optimum efficiency of 14.69% was achieved with the PSC with the film formed using 31 mg/mL MAI/IPA, and the performance curves showed negligible hysteresis, as shown in Fig. 6.

As seen from Fig. 5, the PSC efficiency increases with an increasing PbI_2 thickness up to 200 nm and decreases with 270 nm PbI_2. Figures 7(a)–7(d) show the cross-sectional SEM images of the perovskite films with 85 nm, 150 nm, 200 nm, and 270 nm PbI_2, respectively. These perovskite films are approximately twice as thick as the PbI_2films, agreeing with the previous reports.[65,66] The thickness of the perovskite film increases with an increasing PbI_2 thickness, leading to obviously enhanced ultraviolet-visible absorption between 550 nm to 800 nm, as shown in Fig. 7(e). When the thickness of the perovskite film is less than 400 nm, as shown in Figs. 7(a)–



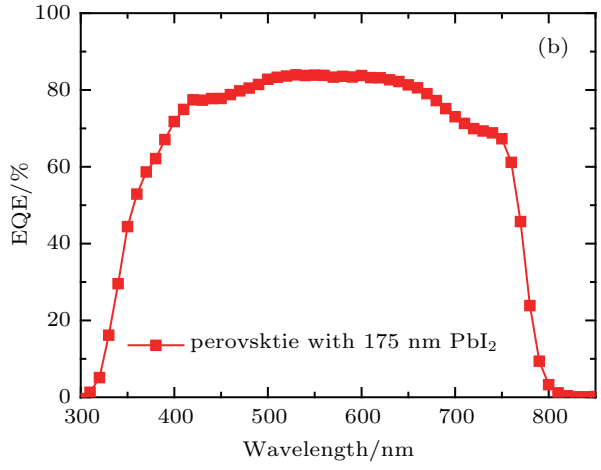


Fig. 6. (color online) Performance of the PSC with 175 nm PbI_2 and 30.5 mg/mL MAI/IPA. (a) J–V curve with an effective area of 0.1 cm^2 and (b) EQE curve of the cell under 1 sun illumination.

7(c), the crystalline grains are perpendicular to the substrates and larger than the film thickness, which are beneficial to transporting photogenerated carriers. For a thicker perovskite film (Fig. 7(d)), the film has a reduced quality with more grain boundaries, resulting in more loss of electricity. Balancing the optical absorption and carrier transport, the optimum thickness of the perovskite film is 400 nm manufactured with 200 nm PbI_2 and 33 mg/mL MAI/IPA. The *J*–*V* curves and performance parameters of the perovskite films of different thicknesses are shown in Fig. 7(f) and Table 2.

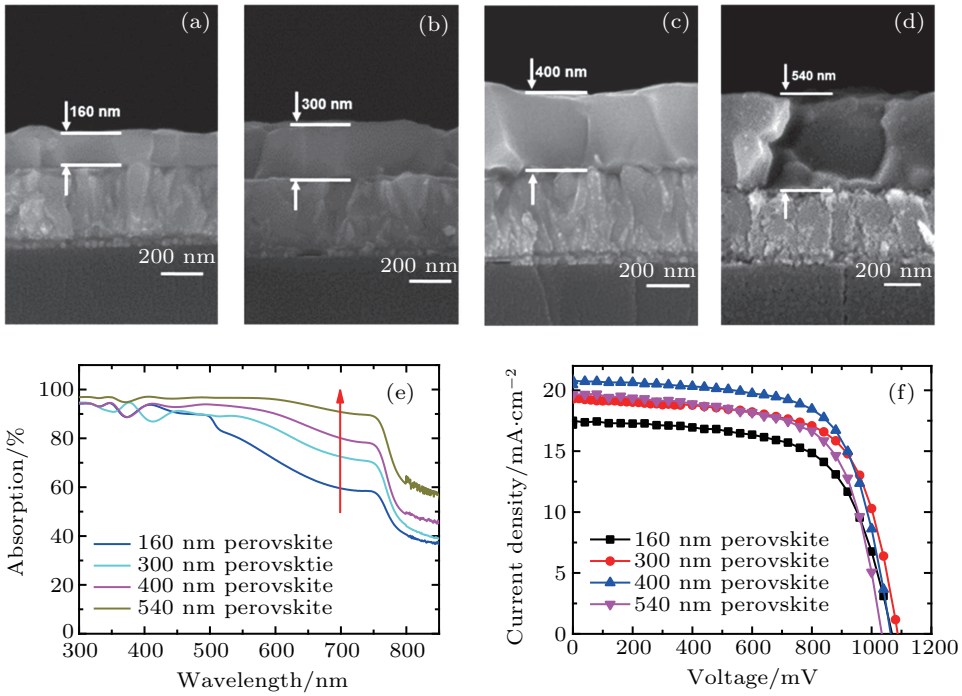


Fig. 7. (color online) SEM images and absorption properties of the perovskite films and performances of the PSCs. SEM cross-sectional images of perovskite films with thicknesses of (a) 160 nm, (b) 300 nm, (c) 400 nm, and (d) 540 nm manufactured by reacting 85 nm, 150 nm, 200 nm, and 270 nm PbI_2 with 16 mg/mL, 27.5 mg/mL, 33 mg/mL, and 46.5 mg/mL MAI/IPA, respectively. (e) Absorption spectra of the perovskite films, and (f) *J*–*V* curves (FB-SC) of the PSCs under 1 sun illumination with different PbI_2 thicknesses matched with the optimal concentrations of MAI/IPA.

Table 2. Performance parameters of the optimal PSCs using different PbI_2 thicknesses reacting with the optimal concentrations of the MAI/IPA solution.

PbI_2 thickness/nm	85	150	200	270
MAI concentration/mg·mL^{-1}	16	27.5	33	46.5
Perovskite thickness/nm	160	300	400	540
J_{sc}/mA·cm^{-2}	17.4	19.3	20.8	19.7
V_{oc}/mV	1060	1090	1060	1020
FF/%	0.642	0.664	0.677	0.663
Maximum Eff./%	11.88	13.99	14.91	13.33

4. Conclusion

We obtained large-grain, pure $CH_3NH_3PbI_3$ using a sequential vacuum deposition, and an efficiency of over 15% was achieved with the PSC fabricated using a sufficient and high pressure of organic MAI vapor. In addition, we investigated the relationship between the inorganic seeding layer thickness and organic molecule concentration to achieve optimum devices using the evaporation–solution method. For the optimum PSC at each PbI_2 thickness, the thickness of the inorganic lead halide and concentration of organic molecule solution showed a linear relationship, and an empirical formula was determined.

Data availability

The data that support the findings of this study are available from the corresponding author on reasonable request.

References

[1] Ponseca Jr C S, Savenije T J, Abdellah M, Zheng K, Yartsev A, Pascher T, Harlang T, Chabera P, Pullerits T, Stepanov A, Wolf J and Sundström V 2014 *J. Am. Chem. Soc.* **136** 5189
[2] Stranks S, Eperon G, Grancini G, Menelaou C, Alcocer M, Leijtens T, Herz L, Petrozza A and Snaith H J 2013 *Science* **342** 341
[3] Gao P, Grätzel M and Nazeeruddin M K 2014 *Energy Environ. Sci.* **7** 2448
[4] Green M A, Ho-Baillie A and Snaith H J 2014 *Nat. Photon.* **8** 506
[5] Correa Baena J P, Steier L, Tress W, Saliba M, Neutzner S, Matsui T, Giordano F, Jacobsson T J, Srimath Kandada A R, Zakeeruddin S M, Petrozza A, Abate A, Nazeeruddin M K, Grätzel M and Hagfeldt A 2015 *Energy Environ. Sci.* **8** 2928
[6] Jesper Jacobsson T, Correa-Baena J P, Pazoki M, Saliba M, Schenk K, Grätzel M and Hagfeldt A 2016 *Energy Environ. Sci.* **9** 1706
[7] Yang Z, Rajagopal A, Chueh C C, Jo S B, Liu B, Zhao T and Jen A K 2016 *Adv. Mater.* **28** 8990
[8] Eperon G E, Leijtens T, Bush K A, Prasanna R, Green T, Wang J T, McMeekin D P, Volonakis G, Milot R L, May R, Palmstrom A, Slotcavage D J, Belisle R A, Patel J B, Parrott E S, Sutton R J, Ma W, Moghadam F, Conings B, Babayigit A, Boyen H, Bent S, Giustino F, Herz L M, Johnston M B, McGehee M D and Snaith H J 2016 *Science* **354** 861
[9] Yin W J, Shi T and Yan Y 2014 *Appl. Phys. Lett.* **104** 063903

[10] Kim J, Lee S H, Lee J H and Hong K H 2014 *J. Phys. Chem. Lett.* **5** 1312

[11] Sutherland B R, Hoogland S, Adachi M M, Kanjanaboos P, Wong C T, McDowell J J, Xu J, Voznyy O, Ning Z, Houtepen A J and Sargent E H 2015 *Adv. Mater.* **27** 53

[12] Malinkiewicz O, Lenes M, Brine H and Bolink H J 2012 *RSC Adv.* **2** 3335

[13] Ono L K, Wang S, Kato Y, Raga S R and Qi Y 2014 *Energy Environ. Sci.* **7** 3989

[14] Burschka J, Pellet N, Moon S J, Humphry-Baker R, Gao P, Nazeeruddin M K and Grätzel M 2013 *Nature* **499** 316

[15] Liu M, Johnston M B and Snaith H J 2013 *Nature* **501** 395

[16] Chen Q, Zhou H, Hong Z, Luo S, Duan H S, Wang H H, Liu Y, Li G and Yang Y 2013 *J. Am. Chem. Soc.* **136** 622

[17] Das S, Yang B, Gu G, Joshi P C, Ivanov I N, Rouleau C M, Aytug T, Geohegan D B and Xiao K 2015 *ACS Photonics* **2** 680

[18] Xiao Z, Bi C, Shao Y, Dong Q, Wang Q, Yuan Y, Wang C, Gao Y and Huang J 2014 *Energy Environ. Sci.* **7** 2619

[19] Chen B, Bai Y, Yu Z, Li T, Zheng X, Dong Q, Shen L, Boccard M, Gruverman A, Holman Z and Huang J 2016 *Adv. Energy Mater.* **6** 1601128

[20] Chen Z, Zhang C, Jiang X F, Liu M, Xia R, Shi T, Chen D, Xue Q, Zhao Y, Su S, Yip H and Cao Y 2017 *Adv. Mater.* **29** 1603157

[21] Wang J, Wang N, Jin Y, Si J, Tan Z, Du H, Cheng L, Dai X, Bai S, He H, Ye Z, Lai M L, Friend R H and Huang W 2015 *Adv . Mater.* **27** 2311

[22] Wu Y, Li J, Xu J Du Y, Huang L, Ni J, Cai H and Zhang J 2016 *RSC Adv.* **6** 16243

[23] Lu H, Tian W, Cao F, Ma Y, Gu B and Li L 2016 *Adv. Funct. Mater.* **26** 1296

[24] Shen L, Fang Y, Wang D, Bai Y, Deng Y, Wang M and Huang J 2016 *Adv. Mater.* **28** 10794

[25] Bi D, Yi C, Luo J, Décoppet J, Zhang F, Zakeeruddin Shaik M, Li X, Hagfeldt A and Grätzel M 2016 *Nat. Energy* **1** 16142

[26] Kakavelakis G, Maksudov T, Konios D, Paradisanos I, Kioseoglou G, Stratakis E and Kymakis E 2017 *Adv. Energy Mater.* **7** 1602120

[27] Tsai H, Nie W, Blancon J C, Stoumpos C C, Asadpour R, Harutyunyan B, Neukirch A J, Verduzco R, Crochet J J, Tretiak S, Pedesseau L, Even J, Alam M A, Gupta G, Lou J, Ajayan P M, Bedzyk M J and Kanatzidis M G 2016 *Nature* **536** 312

[28] You J, Meng L, Song T B, Guo T F, Yang Y M, Chang W H, Hong Z, Chen H, Zhou H, Chen Q, Liu Y, De Marco N and Yang Y 2016 *Nat. Nanotech.* **11** 75

[29] Lin Q, Armin A, Nagiri R C R, Burn P L and Meredith P 2014 *Nat. Photon.* **9** 106

[30] Yang W S, Park B W, Jung E H, Jeon N J, Kim Y C, Lee D U and Seok S I 2017 *Science* **356** 1376

[31] Malinkiewicz O, Yella A, Lee Y H, Espallargas G M, Graetzel M, Nazeeruddin M K and Bolink H J 2013 *Nat. Photon.* **8** 128

[32] Malinkiewicz O, Roldán-Carmona C, Soriano A, Bandiello E, Camacho L, Nazeeruddin M K and Bolink H J 2014 *Adv. Energy Mater.* **4**

[33] Teuscher J, Ulianov A, Muntener O, Gratzel M and Tetreault N 2015 *ChemSusChem* **8** 3847

[34] Gao C, Liu J, Liao C, Ye Q, Zhang Y, He X, Guo X, Mei J and Lau W 2015 *RSC Adv.* **5** 26175

[35] Zhou H, Chen Q and Yang Y 2015 *MRS Bull.* **40** 667

[36] Mao J, Zhang H, He H, Lu H, Xie F, Zhang D, Wong K S and Choy W C H 2015 *RSC Adv.* **5** 73760

[37] Chen C W, Kang H W, Hsiao S Y, Yang P F, Chiang K M and Lin H W 2014 *Adv. Mater.* **26** 6647

[38] Hu H, Wang D, Zhou Y, Zhang J, Lv S, Pang S, Chen X, Liu Z, Padture N P and Cui G 2014 *RSC Adv.* **4** 28964

[39] Bailie C D, Christoforo M G, Mailoa J P, Bowring A R, Unger E L, Nguyen W H, Burschka J, Pellet N, Lee J Z, Grätzel M, Noufi R, Buonassisi T, Salleo A and McGehee M D 2015 *Energy Environ. Sci.* **8** 956

[40] Fu F, Feurer T, Jager T, Avancini E, Bissig B, Yoon S, Buecheler S and Tiwari A N 2015 *Nat. Commun.* **6**

[41] Fu F, Feurer T, Weiss Thomas P, Pisoni S, Avancini E, Andres C, Buecheler S and Tiwari Ayodhya N 2016 *Nat. Energy* **2** 16190

[42] Werner J, Weng C-H, Walter A, Fesquet L, Seif J P, Wolf S D, Niesen B and Ballif C 2015 *J. Phys. Chem. Lett.* **7** 161

[43] Tao C, Neutzner S, Colella L, Marras S, Srimath Kandada A R, Gandini M, Bastiani M D, Pace G, Manna L, Caironi M, Bertarelli C and Petrozza A 2015 *Energy Environ. Sci.* **8** 2365

[44] Ioakeimidis A, Christodoulou C, Lux-Steiner M and Fostiropoulos K 2016 *J. Solid State Chem.* **244** 20

[45] Liu D, Gangishetty M K and Kelly T L 2014 *J. Mater. Chem. A* **2** 19873

[46] Leyden M R, Ono L K, Raga S R, Kato Y, Wang S and Qi Y 2014 *J. Mater. Chem. A* **2** 18742

[47] Chen Y, Chen T and Dai L 2015 *Adv. Mater* **27** 1053

[48] Yang D, Yang Z, Qin W, Zhang Y, Liu S and Li C 2015 *J. Mater. Chem. A* **3** 9401

[49] Werner J, Barraud L, Walter A, Bräuninger M, Sahli F, Sacchetto D, Tétreault N, Paviet-Salomon B, Moon S J, Allebé C, Despeisse M, Nicolay S, De Wolf S, Niesen B and Ballif C 2016 *ACS Energy Lette ACS Energy Lett.* **1** 474

[50] Forgács D, Gil-Escrig L, Pérez-Del-Rey D, Momblona C, Werner J, Niesen B, Ballif C, Sessolo M and Bolink H J 2017 *Adv. Energy Mater.* **7** 1602121

[51] Ahmad S, Kanaujia P K, Niu W, Baumberg J J and Vijaya Prakash G 2014 *ACS Appl. Mater. Interfaces* **6** 10238

[52] Era M, Hattori T, Taira T and Tsutsui T 1997 *Chem. Mater.* **9** 8

[53] Era M, Maeda K and Tsutsui T 1998 *Thin Solid Films* **331** 285

[54] Shi B, Liu, B, Luo J, Li Y, Zheng C, Yao X and Zhang X 2017 *Sol. Energy Mater. Sol. Cells* **168** 214

[55] Fu F, Kranz L, Yoon S, Löckinger J, Jäger T, Perrenoud J, Feurer T, Gretener C, Buecheler S and Tiwari A N 2015 *Physica Status Solidi (a)* **212** 2708

[56] Mahmud M A, Elumalai N K, Upama M B, Wang D, Puthen-Veettil B, Haque F, Wright M, Xu C, Pivrikas A and Uddin A 2017 *Sol. Energy Mater. Sol. Cells* **167** 87

[57] Yang M, Zhang T, Schulz P, Li Z, Li G, Kim D H, Guo N, Berry J J, Zhu K and Zhao Y 2016 *Nat. Commun.* **7** 12305

[58] Zhou H, Chen Q, Li G, Luo S, Song T b, Duan H S, Hong Z, You J, Liu Y and Yang Y 2014 *Science* **345** 542

[59] Song T B, Chen Q, Zhou H, Luo S, Yang Y, You J and Yang Y 2015 *Nano Energy* **12** 494

[60] Ono L K, Leyden M R, Wang S and Qi Y 2016 *J. Mater. Chem. A* **4** 6693

[61] Wang S, Ono L K, Leyden M R, Kato Y, Raga S R, Lee M V and Qi Y 2015 *J. Mater. Chem. A* **3** 14631

[62] Bryant D G P, Troughton J, *et al*. 2014 *Adv. Mater. Interfaces* **26** 7499

[63] Dualeh A, Tétreault N, Moehl T, Gao P, Nazeeruddin M K and Grätzel M 2014 *Adv. Funct. Mater.* **24** 3250

[64] Jiang Q, Chu Z, Wang P, Yang X, Liu H, Wang Y, Yin Z, Wu J, Zhang X and You J 2017 *Adv. Mater.* 1703852

[65] Zhang T, Yang M, Zhao Y and Zhu K 2015 *Nano Lett.* **15** 3959

[66] Im J H, Jang I H, Pellet N, Grätzel M and Park N G 2014 *Nat. Nanotech.* **9** 927